Large-Volume Self-Organization of Polymer/Nanoparticle Hybrids with Millimeter-Scale Grain Sizes Using Brush Block Copolymers

Dong-Po Song,[†] Cheng Li,[†] Nicholas S. Colella,[†] Wanting Xie,[‡] Shengkai Li,[†] Xuemin Lu,[§] Samuel Gido,[†] Jae-Hwang Lee,*[‡] and James J. Watkins*[†]

[†]Department of Polymer Science and Engineering, University of Massachusetts Amherst, 120 Governors Drive, Amherst, Massachusetts 01003, United States

[‡]Department of Mechanical and Industrial Engineering, University of Massachusetts Amherst, 160 Governors Drive, Amherst, Massachusetts 01003, United States

[§]School of Chemistry and Chemical Engineering, Shanghai Jiao Tong University, 800 Dongchuan Road, Shanghai 200240, P. R. China

S *Supporting Information*

ABSTRACT: We report that an exceptionally large volume of highly ordered arrays (single grains) on the order of millimeters in scale can be rapidly created through a unique innate guiding mechanism of brush block copolymers (BBCPs). The grain volume is over 10^9 times larger than that of typical self-assembled linear BCPs (LBCPs). The use of strong interactions between nanoparticles (NPs) and BBCPs enables high loadings of functional materials, up to 76 wt % (46 vol %) in the target domain, while maintaining excellent long-range order. Overall, this work provides a simple method to precisely control the spatial orientation of functionalities at nanometer length scales over macroscopic volumes, thereby enabling the production of hybrid materials for many important applications.

The organization of functional nanomaterials, such as semiconductor, plasmonic, and dielectric nanoparticles (NPs), over macroscopic volumes using low-cost "bottom up" methods is highly desirable for the development of next-generation electric, optical, energy-harvesting, and memory devices.[1,2] However, the lack of sufficient long-range order in self-assembled nanostructures is a bottleneck for many nanotechnology applications. The rapid fabrication of functional nanocomposites with precise control over the organization of periodic NP arrays has remained a significant challenge.

Conventional self-assembly methods, including the application of linear block copolymers (LBCPs), are limited by the slow kinetics of the self-assembly process, poor long-range alignment of nanostructures, and limited loading of NPs.[3–14] Kinetically trapped morphologies (i.e., large defects) are often created in nanocomposites during the self-assembly process, especially for samples containing high loadings of NPs.[11,14] Polymer chain entanglements of LBCPs and entropic penalties associated with NP incorporation lead to severe barriers to well-ordered composite materials. As a result, well-aligned NP arrays are achievable only within very small volume elements on the order of micrometer scale,[4–14] which is a barrier for future

practical use. While rapid progress has been realized in achieving the long-range organization of neat BCP thin films using topographical,[15] chemical,[16] mechanical,[17] thermal,[18] and electric-field guiding[19] and some work has demonstrated the potential of organizing bulk LBCP films using magnetic fields,[20] these external guiding methods generally require sophisticated precedures or very strong fields, which are time-consuming and high-cost when fabricating large areas of well-ordered materials. To date, no macroscopic ordering of BCPs without external guiding forces has been reported.

In nature, minor changes in the chemical structures of biological macromolecules can have a significant influence on their self-assembled structures and functionalities, such as protein folding and misfolding.[21] For the synthetic macromolecules, BCPs, chemists have made breakthroughs in the design and synthesis of brush block copolymers (BBCPs).[22–24] Benefiting from their rigid molecular structure, these BBCPs exhibit substantially reduced polymer chain entanglements relative to their linear analogues. We previously conducted initial feasibility studies using BBCPs as templates for the controlled self-assembly of NPs.[25] However, the potential benefits of BBCPs for large-volume organization of NPs on a macroscopic scale were not realized. Further tailoring of the BBCP molecular structure is of great interest to create macromolecular building blocks, also known as "molecular Lego", that can afford stable supramolecular architectures with long-range directional order.

Here we demonstrate the long-range order formed through the self-assembly of rationally designed BBCPs without external guiding. Two important factors were taken into consideration for the molecular design of the BBCPs. First, the molecular backbone is highly stretched by using bulky side chains to greatly decrease polymer chain entanglements. Second, amphiphilic side chains with low glass transition temperatures are employed to enhance the microphase segregation at relatively low temperatures. Specifically, the BBCPs are (polynorbornene-*graft*-poly(*tert*-butyl acrylate))-*block*-(polynorbornene-*graft*-poly(ethylene oxide)) (($PNB-PtBA_{8.2k}$)$_n$-*b*-

(PNB−PEO$_{5k}$)$_m$, denoted as PtBA-*b*-PEO for brevity) synthesized by sequential ring-opening metathesis polymerization (ROMP) (see the Supporting Information for details and Figures S1−S6 and Table S1 for characterization data). In comparison with the (polynorbornene-*graft*-polystyrene)-*block*-(polynorbornene-*graft*-poly(ethylene oxide)) (PS$_{3.5k}$-*b*-PEO$_{2k}$) BBCP system used in the previous studies,[25] several improvements were made in the molecular design of the side chains, including more steric hindrance (PtBA > PS), higher molecular weights (MWs), and a lower glass transition temperature of the PtBA block (see the molecular structure in Figure 1a). Highly
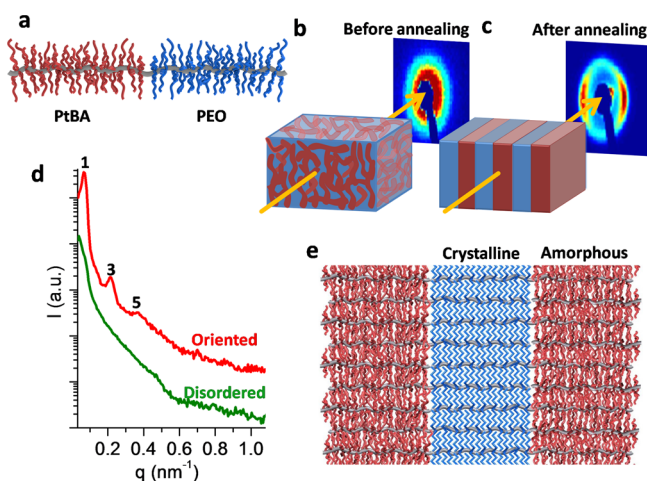

Figure 1. Macroscopic orientation via rapid self-assembly of PtBA-*b*-PEO BBCPs. (a) Molecular illustration of the BBCPs. (b, c) 2D SAXS patterns of BBCP-**A** (M_n = 1850 kg/mol, f_{PEO} = 48.4%) before and after annealing at 110 °C for 5 min. (d) 1D SAXS profiles of BBCP-**A** before (disordered) and after annealing (oriented). (e) Proposed molecular packing of the BBCPs in the highly ordered lamellar nanostructure.

oriented nanostructures were generated within a few minutes via self-assembly of PtBA-*b*-PEO BBCPs upon thermal annealing, as indicated by two-dimensional small-angle X-ray scattering (2D SAXS) (Figure 1b vs Figure 1c). For comparison, no such anisotropic structure was observed for the PS-*b*-PEO BBCPs after thermal annealing (Figure S7).[25b] The 1D SAXS profile of the sample after annealing (Figure 1d) shows a primary scattering peak at a scattering vector (q) of 0.065 nm^{-1}, indicating a domain spacing of approximately 97 nm ($d = 2\pi/q$). A well-ordered lamellar structure is confirmed by the higher-order reflections located at $3q$ and $5q$.

In comparison with LBCPs, BBCPs have a rigid backbone along the polymer chain and fewer chain entanglements. Therefore, the BBCP molecules can self-assemble into the well-ordered lamellar structure in a short time scale upon annealing. The MW of (PNB−PtBA$_{8.2k}$)$_{116}$-*b*-(PNB−PEO$_{5k}$)$_{179}$ (BBCP-**A**) is 1850 kg/mol, which is several orders of magnitude larger than those of the previous LBCP systems that can be aligned using external guiding methods,[15−20] providing accessibility to large-period composites. Although additional work is required to fully understand the molecular packing in the well-ordered lamellar structure and its role in the kinetics of assembly, the highly elongated nature of the BBCP molecules normal to the intermaterial dividing surface of PtBA/PEO domains virtually eliminated entanglements and thus led to the very rapid ordering kinetics (Figure 1e).[24] In addition to the molecular rigidity, PEO crystallization is another potential factor that

could contribute to the ordering of the BBCPs. Crystallization of the PEO block was confined to the PEO domains, as confirmed by polarized optical microscopy images, in which large, uniform colored areas were observed under crossed polarizers (Figure S8). However, anisotropic 2D SAXS patterns (Figure S9) were also observed at temperatures above the melting point of PEO (Figure S6), indicating that the preordered structure with the PEO crystallization can be persistent over the melting temperature of PEO because of the interfacial energy of PEO and PtBA but that the effect of the PEO crystallization can be less significant for the long-range order (see below). Further studies are needed to fully understand the detailed mechanism of long-range ordering.

To further verify that the highly ordered lamellar structure is nearly an equilibrium configuration rather than a kinetically trapped state, we carried out in situ SAXS measurements on a polymer sample first by heating and cooling stepwise and then by multiple direct heating−cooling cycles. The long-range order decreased as the temperature was increased to 110 °C but was regained when temperature was decreased to 25 °C (Figure S9a). This was further characterized by analyzing the X-ray scattering intensity as a function of azimuthal angle at various temperatures (Figure S10). 1D SAXS (Figure S11a) revealed enhanced phase separation after the stepwise annealing process, as indicated by the disappearance of the broad peak and the appearance of higher-order peaks. The highly oriented structure was very stable during the subsequent multiple heating−cooling cycles, as shown in Figures S9b and S11b, suggesting that the morphology approached an equilibrium structure.

We also investigated the layer orientation in different regions of the polymer sample and obtained a map of local orientations by continuous SAXS scan measurements. Figure 2a shows the orientation map of a centered large area (3.08 mm × 3.06 mm). Each arrow or plus mark in the map represents a SAXS measurement of an area as large as 0.22 mm × 0.18 mm, which was the area of the X-ray beam. The arrow direction (layer

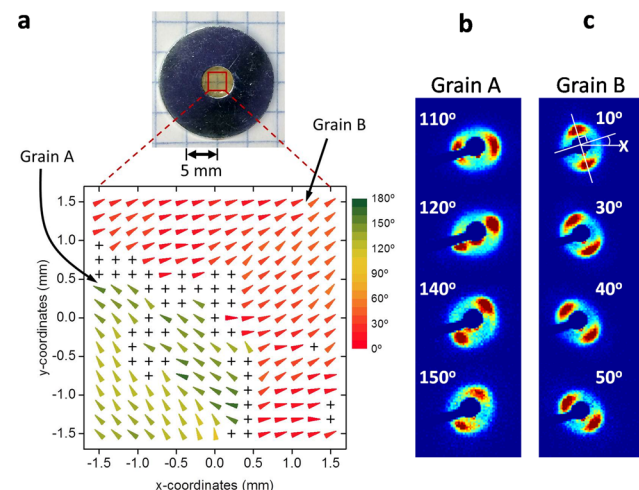**Figure 2.** Mapping of the layer orientation in BBCP-**A** (M_n = 1850 kg/mol, f_{PEO} = 48.4%) using continuous SAXS scan measurements. The thickness of the sample was approximately 0.66 mm. (a) Orientation map of an area as large as 3.08 mm × 3.06 mm. (b, c) Representative 2D SAXS patterns with different azimuthal angles in grains A and B. The azimuthal angle of 2D SAXS parallel to the *x* direction is defined as 0°. The smaller angle between the layer and the *x* axis is defined as the layer orientation in the map.

orientation) is normal to the 2D SAXS pattern (see the representative 2D SAXS patterns in Figure 2b,c) and was determined on the basis of the azimuthal angle. Each plus mark represents a region where at least two orientations exist. All of the 2D SAXS patterns corresponding to the data points in the map can be found in Figure S12. Adjacent data points with a difference in azimuthal angle briefly less than 20° are defined to be in the same grain. As shown in Figure 2a, it is evident that there are two different grains A and B as well as boundaries (plus marks); grain A shows a layer orientation between 110° and 150°, corresponding to 2D SAXS patterns with azimuthal angles between 20° and 60°, while the orientation of layers in grain B is confined between 10° and 50°, corresponding to azimuthal angles between 100° and 140°. There are up to 135 data points in grain B, corresponding to an area as large as 5.40 mm^2 and a volume of 3.56 mm^3, which is over 10^9 times larger than the grain sizes of self-assembled LBCPs.[3] In addition, 3D SAXS measurements were further conducted on a piece of sample from a selected area of a rectangle in grain B and indicated good alignment of the lamellar structure (see Figure S13).

The BBCP system was further used as a template to control the spatial orientation of NP arrays, and gold NPs with a core diameter of approximately 2 nm and 4-mercaptophenol ligands were chosen as a model system for the investigation (see the transmission electron microscopy (TEM) micrograph in Figure S14). For the BBCP–NP composites, we typically prepared 2% (w/v) polymer solutions in anhydrous tetrahydrofuran (THF) admixed with various amounts of gold NPs, resulting in different weight percentages in the solid. Herein the weight percentage (wt %) of NPs in the composites is based on the mass of the NP core and ligand shell, while the volume percentage (vol %) of NPs (core + ligand) can be estimated using the thermogravimetric analysis (TGA) data and the densities of the components (Table S2 and Figure S15). Strong H-bonding interactions between the ligands on the gold NPs and the PEO brushes of the PtBA-b-PEO BBCPs enabled selective incorporation and high loading of the gold NPs into the PEO domains (see Figure 3a). As shown in Figure 3b, a symmetric lamellar morphology of BBCP-**A** was observed, as confirmed by the higher-order peaks at $3q$ and $5q$, while an asymmetric lamellar structure was formed in the composite samples containing over 40 wt % (15 vol %) gold NPs, as indicated by the peaks at $2q$ and $4q$. The asymmetric lamellar structure was due to swelling of the PEO domains by the NP additives. The domain spacing increased from 97 to 125 nm as the NP loading increased from 0 to 60 wt % (29 vol %). Most impressively, highly oriented lamellar morphologies of the NP arrays (Figure 3c) were observed even at an ultrahigh NP loading of up to 60 wt %, corresponding to 76 wt % (46 vol %) in the PEO domain, suggesting that the rapid and long-range ordering of our BCP systems was maintained in the presence of a large amount of gold NPs. The long-range orientation was further confirmed by 2D SAXS with the X-ray beam incident to both the top surface and the side of a blend containing 50 wt % (22 vol %) gold NPs (Figure S16). Nearly the same orientation of NP layers was observed when the sample was turned by 90° along the longitudinal axis of the sample, indicative of good orientation. Wide-angle X-ray scattering (WAXS) was employed to investigate the influence of the NP loading on the PEO crystallization (Figure S17). No considerable crystalline PEO was found in the composite samples containing >50 wt % gold NPs, so the long-range order of these samples
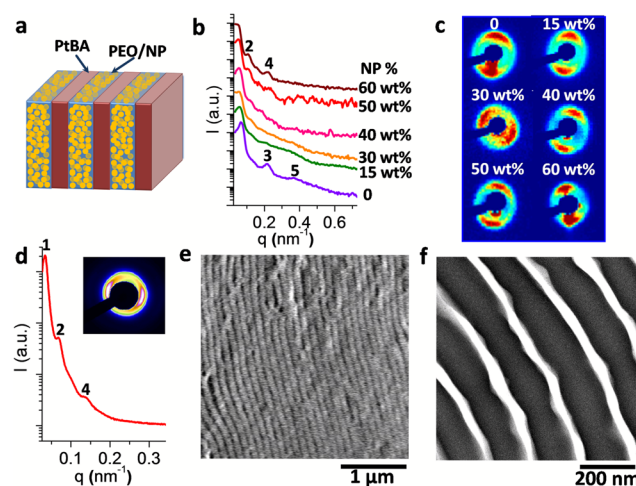

Figure 3. Nanocomposites based on PtBA-b-PEO BBCPs containing highly oriented gold NP arrays. (a) Illustration of the highly ordered NP arrays selectively incorporated into the PEO domains via H-bonding interactions. (b) 1D SAXS profiles of blends of BBCP-**A** with different loadings of gold NPs, including 15 wt % (4.6 vol %), 30 wt % (11 vol %), 40 wt % (15 vol %), 50 wt % (22 vol %), and 60 wt % (29 vol %). (c) Anisotropic 2D SAXS patterns corresponding to the 1D SAXS profiles in (b). (d) 1D and 2D SAXS data for a blend of BBCP-**B** (M_n = 2694 kg/mol, f_{PEO} = 48.4%) with 50 wt % gold NPs, indicating a domain spacing of up to 188 nm. (e, f) Cross-sectional (e) FESEM and (f) TEM micrographs of the composite sample based on BBCP-**B**.

suggests that the molecular rigidity and the strong phase segregation (rather than PEO crystallization) are possibly the dominant internal driving forces for the orientation.

The highly oriented NP arrays were also observed in a blend of BBCP-**B** with a higher MW (M_n = 2694 kg/mol) (Figure 3d). As shown in Figure 3e,f, the well-ordered lamellar morphology was confirmed by field-emission scanning electron microscopy (FESEM) and TEM. The high loading of the gold NPs selectively within PEO domains and the wide lattice spacing (188 nm) provided a good contrast for cross-sectional imaging of the composite samples without staining. Figure 3e shows a representative cross-sectional FESEM micrograph of the blend of BBCP-**B** with 50 wt % (22 vol %) gold NPs. A highly oriented lamellar morphology was observed, consistent with the SAXS results (Figure 3d). Figure 3f shows a TEM micrograph of the microtomed sample indicating an asymmetric lamellar morphology with the gold NPs appearing as the dark regions, consistent with the FESEM and SAXS results. We note that since PtBA and PEO of the unstained samples have similar electron densities, the contrast observed in the TEM image is evidently due to the gold NPs residing exclusively in PEO domains, as illustrated by Figure 3a. TEM micrographs of blends containing different loadings of gold NPs can be found in Figure S18, and FESEM micrographs of a larger cryofractured surface are shown in Figure S19. The domain spacing of the aligned NP arrays was widely tunable from 110 to 188 nm simply by changing the loading of the NPs or the MW of the BBCP (Figure 3). The innate guiding mechanism of the BBCP system enables the fabrication of novel hybrid nanomaterials with the long-range order of functional building blocks within large volume elements, providing a material platform for the investigation of integrated plasmonic, nonlinear optical, and electric properties arising from the long-range arrangements.

In summary, many applications in nanotechnology will require the precise alignment of functional nanomaterials on a macroscopic scale. In this work, we have shown that macroscopic ordering can be readily achieved through the innate guiding of self-assembly of BBCPs with large steric hindrance and a low glass transition temperature of the side chains. More importantly, the long-range order was maintained in the presence of high loadings of functional additives such as gold NPs, providing a simple strategy for the long-range alignment of a wide range of potential functional additives such as small molecules, quantum dots, anisotropic NPs, magnetic NPs, etc. The well-aligned NP arrays may serve as novel materials for the fabrication of high-performance polarizing filters and plasmonic or nonlinear optical devices. The ultrafast kinetics of ordering offers new opportunities for rapid, low-cost, and scalable manufacturing.

ASSOCIATED CONTENT

Ⓢ Supporting Information

The Supporting Information is available free of charge on the ACS Publications website at DOI: 10.1021/jacs.5b08632.

Experimental information and supplementary figures (PDF)

AUTHOR INFORMATION

Corresponding Authors

*watkins@polysci.umass.edu
*leejh@umass.edu

Notes

The authors declare no competing financial interest.

ACKNOWLEDGMENTS

REFERENCES

(1) (a) Talapin, D. V.; Lee, J.-S.; Kovalenko, M. V.; Shevchenko, E. V. *Chem. Rev.* **2010**, *110*, 389. (b) Huynh, W. U.; Dittmer, J. J.; Alivisatos, A. P. *Science* **2002**, *295*, 2425. (c) Lopes, W. A.; Jaeger, H. M. *Nature* **2001**, *414*, 735. (d) De Rosa, C.; Auriemma, F.; Di Girolamo, R.; Pepe, G. P.; Napolitano, T.; Scaldaferri, R. *Adv. Mater.* **2010**, *22*, 5414. (e) Briseno, A. L.; Yang, P. *Nat. Mater.* **2009**, *8*, 7.

(2) Orilall, M. C.; Wiesner, U. *Chem. Soc. Rev.* **2011**, *40*, 520.

(3) Ryu, H. J.; Fortner, D. B.; Lee, S.; Ferebee, R.; De Graef, M.; Misichronis, K.; Avgeropoulos, A.; Bockstaller, M. R. *Macromolecules* **2013**, *46*, 204.

(4) Kao, J.; Thorkelsson, K.; Bai, P.; Rancatore, B. J.; Xu, T. *Chem. Soc. Rev.* **2013**, *42*, 2654.

(5) Bockstaller, M. R.; Lapetnikov, Y.; Margel, S.; Thomas, E. L. *J. Am. Chem. Soc.* **2003**, *125*, 5276.

(6) Chiu, J. J.; Kim, B. J.; Kramer, E. J.; Pine, D. J. *J. Am. Chem. Soc.* **2005**, *127*, 5036.

(7) Lin, Y.; Böker, A.; He, J. B.; Sill, K.; Xiang, H. Q.; Abetz, C.; Li, X. F.; Wang, J.; Emrick, T.; Long, S.; Wang, Q.; Balazs, A.; Russell, T. P. *Nature* **2005**, *434*, 55.

(8) Balazs, A. C.; Emrick, T.; Russell, T. P. *Science* **2006**, *314*, 1107.

(9) Lin, Y.; Daga, V. K.; Anderson, E. R.; Gido, S. P.; Watkins, J. J. *J. Am. Chem. Soc.* **2011**, *133*, 6513.

(10) Jang, S. G.; Kramer, E. J.; Hawker, C. J. *J. Am. Chem. Soc.* **2011**, *133*, 16986.

(11) Jang, S. G.; Khan, A.; Hawker, C. J.; Kramer, E. J. *Macromolecules* **2012**, *45*, 1553.

(12) Warren, S. C.; Messina, L. C.; Slaughter, L. S.; Kamperman, M.; Zhou, Q.; Gruner, S. M.; DiSalvo, F. J.; Wiesner, U. *Science* **2008**, *320*, 1748.

(13) Zhao, Y.; Thorkelsson, K.; Mastroianni, A. J.; Schilling, T.; Luther, J. M.; Rancatore, B. J.; Matsunaga, K.; Jinnai, H.; Wu, Y.; Poulsen, D.; Fréchet, J. M. J.; Alivisatos, A. P.; Xu, T. *Nat. Mater.* **2009**, *8*, 979.

(14) Kao, J.; Xu, T. *J. Am. Chem. Soc.* **2015**, *137*, 6356.

(15) (a) Bita, I.; Yang, J. K. W.; Jung, Y. S.; Ross, C. A.; Thomas, E. L.; Berggren, K. K. *Science* **2008**, *321*, 939. (b) Park, S.; Lee, D. H.; Xu, J.; Kim, B.; Hong, S. W.; Jeong, U.; Xu, T.; Russell, T. P. *Science* **2009**, *323*, 1030.

(16) Stoykovich, M. P.; Müller, M.; Kim, S. O.; Solak, H. H.; Edwards, E. W.; de Pablo, J. J.; Nealey, P. F. *Science* **2005**, *308*, 1442.

(17) Angelescu, D. E.; Waller, J. H.; Adamson, D. H.; Deshpande, P.; Chou, S. Y.; Register, R. A.; Chaikin, P. M. *Adv. Mater.* **2004**, *16*, 1736.

(18) (a) Berry, B. C.; Bosse, A. W.; Douglas, J. F.; Jones, R. L.; Karim, A. *Nano Lett.* **2007**, *7*, 2789. (b) Majewski, P. W.; Yager, K. G. *ACS Nano* **2015**, *9*, 3896.

(19) Liedel, C.; Schindler, K. A.; Pavan, M. J.; Lewin, C.; Pester, C. W.; Ruppel, M.; Urban, V. S.; Shenhar, R.; Böker, A. *Small* **2013**, *9*, 3276.

(20) (a) Majewski, P. W.; Gopinadhan, M.; Osuji, C. O. *J. Polym. Sci., Part B: Polym. Phys.* **2012**, *50*, 2. (b) Gopinadhan, M.; Majewski, P. W.; Beach, E. S.; Osuji, C. O. *ACS Macro Lett.* **2012**, *1*, 184.

(21) Dobson, C. M. *Nature* **2003**, *426*, 884.

(22) Rzayev, J. *Macromolecules* **2009**, *42*, 2135.

(23) (a) Xia, Y.; Olsen, B. D.; Kornfield, J. A.; Grubbs, R. H. *J. Am. Chem. Soc.* **2009**, *131*, 18525. (b) Sveinbjörnsson, B. R.; Weitekamp, R. A.; Miyake, G. M.; Xia, Y.; Atwater, H. A.; Grubbs, R. H. *Proc. Natl. Acad. Sci. U. S. A.* **2012**, *109*, 14332. (c) Macfarlane, R. J.; Kim, B.; Lee, B.; Weitekamp, R. A.; Bates, C. M.; Lee, S. F.; Chang, A. B.; Delaney, K. T.; Fredrickson, G. H.; Atwater, H. A.; Grubbs, R. H. *J. Am. Chem. Soc.* **2014**, *136*, 17374.

(24) Gu, W.; Huh, J.; Hong, S. W.; Sveinbjornsson, B. R.; Park, C.; Grubbs, R. H.; Russell, T. P. *ACS Nano* **2013**, *7*, 2551.

(25) (a) Song, D.-P.; Lin, Y.; Gai, Y.; Colella, N. S.; Li, C.; Liu, X.-H.; Gido, S.; Watkins, J. J. *J. Am. Chem. Soc.* **2015**, *137*, 3771. (b) Song, D.-P.; Li, C.; Colella, N. S.; Lu, X.; Lee, J.-H.; Watkins, J. J. *Adv. Opt. Mater.* **2015**, *3*, 1169.